Programming Palladium Cage Geometry through Ligand Redox Modulation

Jennifer Bou Zeid, Jean Nicolas, Maksym Dekhtiarenko, David Canevet, Magali Allain, Vincent Carré, Frédéric Aubriet, Laura Neukirch, Elie Benchimol, Marc Sallé, et al.

Angewandte Chemie

Angewandte Chemie

Zitierweise: *Angew. Chem. Int. Ed.* **2026**, e5709785
doi.org/10.1002/anie.5709785

FORSCHUNGSARTIKEL OPEN ACCESS

Programming Palladium Cage Geometry through Ligand Redox Modulation

Jennifer Bou Zeid[1] | Jean Nicolas[1] | Maksym Dekhtiarenko[1] | David Canevet[1] | Magali Allain[1] | Vincent Carré[2] | Frédéric Aubriet[2] | Laura Neukirch[3] | Elie Benchimol[3] | Marc Sallé[1] | Guido H. Clever[3] | Sébastien Goeb[1]

[1]Univ Angers, CNRS, MOLTECH-ANJOU, Angers, France | [2]Université De Lorraine, LCP-A2MC, Metz, France | [3]Department of Chemistry and Chemical Biology, TU Dortmund University, Dortmund, Germany

Correspondence: Marc Sallé (marc.salle@univ-angers.fr) | Guido H. Clever (guido.clever@tu-dortmund.de) | Sébastien Goeb (sebastien.goeb@univ-angers.fr)

Received: 13 February 2026 | **Revised:** 1 April 2026 | **Accepted:** 17 April 2026

Keywords: coordination cages | exTTF | redox | self-assembly | stimuli-induced transformations

ABSTRACT

Incorporating redox active ligands into coordination cages offers a direct way to reach architectures whose structure or composition can be modulated in response to changes in the oxidation state. An exTTF-based ditopic ligand L affords a M_2L_4 cage in presence of a palladium(II) salt (M). The resulting M_2L_4 cavity exhibits selective binding properties for medium length α,ω-dinitrile alkanes. Modifying the coordination geometry of the ligand by oxidation to its L^{ox} state redirects the self-assembly process toward a $M_2L^{ox}{}_2$ structure. The oxidized ligand can also be combined with a dibenzothiophene linker (L′) to afford a heteroleptic $M_2L^{ox}L'_2$ structure whose vacant coordination sites enable subsequent dimerization into an unprecedented $M_4L_4L'_4$ architecture. Key intermediates and products were structurally authenticated by single-crystal x-ray diffraction. Notably, these processes are reversible. Reduction converts the $M_2L^{ox}L'_2$ assembly back to the homoleptic M_2L_4 cage. This sequence illustrates how changes of oxidation state can reshape nuclearity and composition in metal organic assemblies.

1 | Introduction

The metal directed self-assembly strategy provides an efficient route to well-defined discrete metalla-organic architectures whose shape is controlled by the coordination preferences of the metal center and the geometry of the organic linkers [1–6]. Palladium(II)-based assemblies have played a central role in this field because their square planar geometry supports a rather predictable structure formation, often under thermodynamic control [7–11]. These properties have enabled the development of a large variety of cavities with a good propensity for guest binding [12–14], e.g., for the stabilization of reactive species [15] or applications in catalysis [16–22], purification [23–28] or molecular delivery [29–31].

Recent efforts have been dedicated to the control of structural complexity in such assemblies. The large majority of early cages were homoleptic, i.e., built from a single type of ligand. The emergence of heteroleptic analogs, i.e., assemblies incorporating two or more different ligands, opens new opportunities in the field. Indeed, the self-assembly of ligands with different geometries may result in asymmetric cavities, while the introduction of complementary functionalities within a single architecture becomes possible [14, 32–44]. Such features are particularly attractive for introducing directionality, multifunctionality, or differentiated reactivity. Nevertheless, the formation of such heteroleptic structures is often limited by winning control over underlying self-sorting processes, that may favor homoleptic products or the formation of statistical mixtures. Strategies based on shape

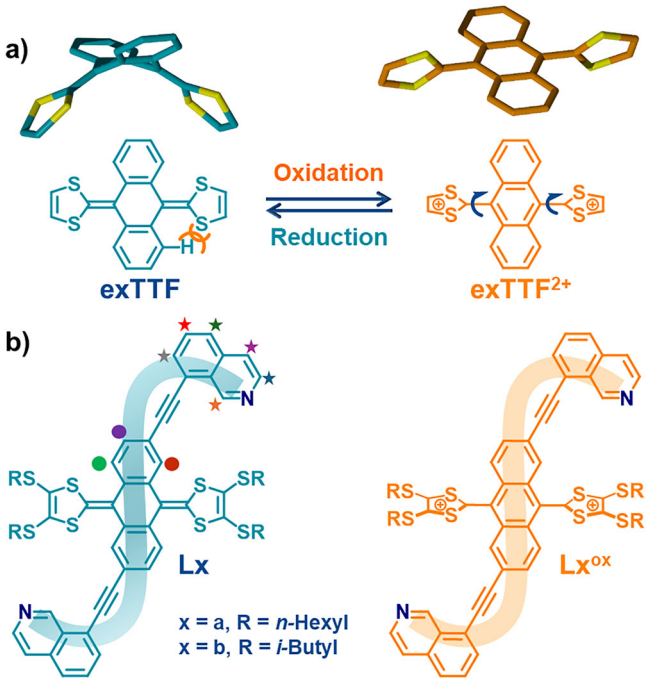

FIGURE 1 | (a) The exTTF moiety and the associated reversible geometric changes occurring along the two-electron redox process and (b) the structure of ligand **L** in its neutral and oxidized state (**x** in **Lx**, stems for the R substituent, i.e., **La** and **Lb**).

complementary assembly, coordination sphere engineering and adjacent backbone interactions have been developed to address this constraint and have since allowed to uncover a variety new structural motif [37, 45, 46].

In parallel, the dynamic nature of the metal ligand bonds allows coordination cages to reorganize when exposed to external stimuli [47–52]. Recent studies describe transformable systems that respond to addition of a competitive ligand [53–55] or a guest molecule [56–58], concentration [59–61], solvent [62] or temperature changes [63], pH modulation [64, 65] or light irradiation [66, 67]. As a result, both the geometry of the cage and its associated functions can be tuned in a stimulus-dependent manner.

On this basis, redox active ligands offer additional opportunities [68–73] since modulation of the oxidation state affects the charge distribution and, in some specific cases, the geometry of the ligand. Therefore, such process may redefine the coordination profile and change the geometry of the corresponding assemblies, offering new structural possibilities [74–76]. Only few examples have explored the redox state of the ligand to drive the formation or rearrangement towards new discrete metalla-based assemblies [76–78]. In this context, the so-called exTTF scaffold (exTTF: 2-[9-(1,3-dithiol-2-ylidene)anthracen10(9H)-ylidene]-1,3-dithiole) [79–81] is a particularly promising building block to consider when designing a ligand, given the drastic conformational changes that occur upon its oxidation to the dicationic state (Figure 1a).

We describe hereafter a ditopic exTTF-based ligand **L** and its self-assembly with palladium(II) cations to afford a $\mathbf{Pd_2L_4}$ homoleptic

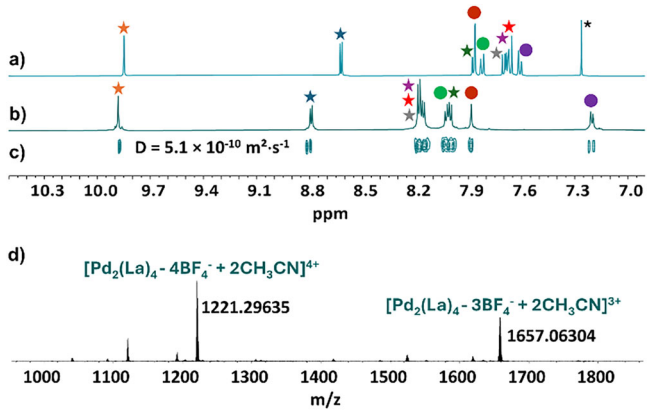

FIGURE 2 | ^{1}H NMR spectra (see Figure 1b for ^{1}H NMR assignments) of (a) ligand **La** in chloroform-d_3, (b) cage $\mathbf{Pd_2(La)_4}$ in acetonitrile-d_3 at C = 0.7 mM, (c) corresponding ^{1}H DOSY NMR and (d) ESI-FTICR HRMS spectrum of cage $\mathbf{Pd_2(La)_4}$ recorded in acetonitrile at 0.07 mM.

cage. This structure displays selective host-guest recognition properties towards α,ω-dinitrile alkane derivatives. Interestingly, a different L/M stoichiometry is obtained upon associating the dicationic oxidized version of **L**, i.e., $\mathbf{L^{ox}}$, which provides a $\mathbf{Pd_2(L^{ox})_2}$ twisted ring structure. $\mathbf{L^{ox}}$ was also combined with a dibenzothiophene-based linker **L′**, to produce a heteroleptic $\mathbf{Pd_2(L^{ox})(L')_2}$ species. Interestingly, reduction of the latter assembly regenerates the homoleptic $\mathbf{Pd_2L_4}$ cage, illustrating the possibility to switch between heteroleptic and homoleptic architectures, through a redox stimulus. Finally, an unprecedented dimeric $\mathbf{Pd_4(L^{ox})_4(L')_4}$ structural motif was also characterized through x-ray diffraction.

2 | Results and Discussion

The bis-functionalized electron-rich exTTF based ligand **L** was designed as two variants, **La** and **Lb**, that share the same overall structure and differ only by the nature of their alkyl substituents, i.e., *n*-hexyl chains in **La** and isobutyl chains in **Lb** (Figure 1b). The introduction of hexyl chains was intended to ensure good solubility of the resulting assemblies, while the isobutyl analogue was synthesized as this substituent previously showed a higher propensity to promote crystallization [76].

Both were obtained through a Horner Wadsworth Emmons reaction between 2,6-dibromoanthraquinone and the appropriate phosphonate ester (**1a** or **1b**) [76, 82], affording the exTTF core, followed by Sonogashira coupling reactions with ethynyl-isoquinoline **3** (Figure S1) [83].

Both ligands were then combined with a Pd(II) salt to assess their capacity to form the expected M_2L_4 assemblies. Reactions of **La** or **Lb** with $[Pd(CH_3CN)_4](BF_4)_2$ in acetonitrile at 50°C for 12 h produced a single discrete species in each case. The formation of discrete self-assemblies was confirmed by ^{1}H and ^{1}H DOSY NMR experiments, with well-defined spectra and an identical diffusion coefficient $D = 5.1 \times 10^{-10}$ m^2·s^{-1} (Figure 2a–c for **La** and S17–S19 for **Lb**). This value corresponds to a hydrodynamic radius r_H = 12.3 Å, as determined from the Stokes-Einstein

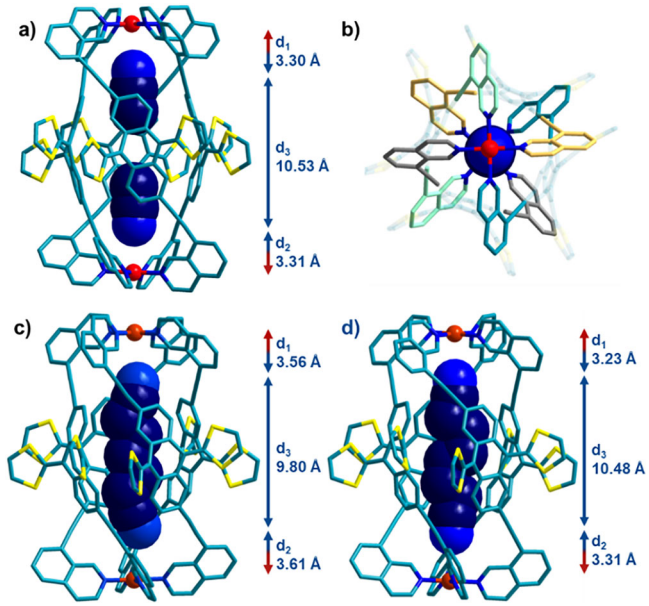

FIGURE 3 | X-Ray crystal structures of (a, b) $\mathbf{Pd_2(Lb)_4}$ featuring two guest CH_3CN molecules, (c) $\mathbf{C_7}\subset\mathbf{Pd_2(Lb)_4}$ and (d) $\mathbf{C_8}\subset\mathbf{Pd_2(Lb)_4}$. In all cases, the *M*,*M*-helicity enantiomer is shown.

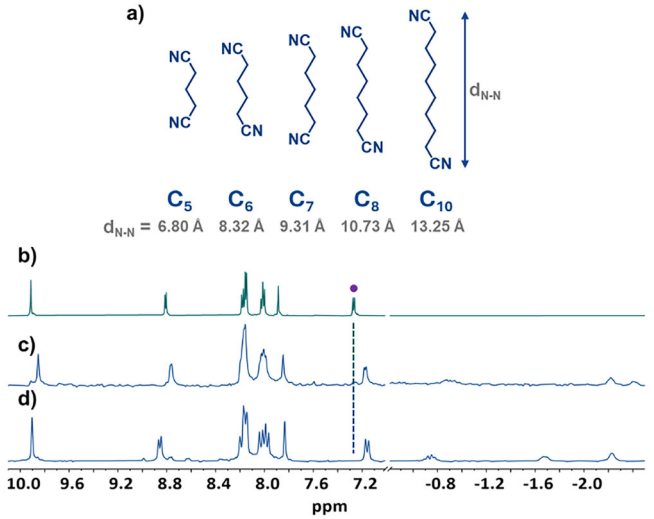

FIGURE 4 | (a) α,ω-Dinitrile alkane substrates with their respective *N-N* intramolecular distances extracted from MM^+ simulations and ^1H NMR spectra in acetonitrile-d_3 at C = 0.35 mM of (b) cage $\mathbf{Pd_2(Lb)_4}$ (see assignment on Figure 2b in the case of cage $\mathbf{Pd_2(La)_4}$), (c) cage $\mathbf{Pd_2(Lb)_4}$ + 80 equiv. of $\mathbf{C_7}$ and (d) cage $\mathbf{Pd_2(Lb)_4}$ + 2 equiv. of $\mathbf{C_8}$.

equation, a value which is consistent with the expected M_2L_4 formulation.

HRMS Analyses further support the formation of Pd_2L_4 cages for both systems (Figures 2d, S16 for **La** and S20 for **Lb**), revealing sets of peaks corresponding to charged adducts featuring two acetonitrile molecules and characteristic of 4^+ and 3^+ species. The latter arise from the partial loss of BF_4^- counter-anions and the observed isotopic distributions match closely those calculated for the proposed M_2L_4 formulations.

While no suitable single crystals of $\mathbf{Pd_2(La)_4}$ could be obtained, crystals of the isobutyl analogue $\mathbf{Pd_2(Lb)_4}$ were successfully grown by vapor diffusion of ethyl acetate over a solution of the cage in acetonitrile in the presence of tetrabutylammonium perrhenate ($TBAReO_4$). X-Ray diffraction (Figure 3a, b) reveals that the isoquinoline units adopt twisted conformations to satisfy the square-planar coordination environment, resulting in a helicate structure with both *ΔΔ* (*M*) and *ΛΛ* (*P*) enantiomers present in the unit cell. Noteworthy, two acetonitrile molecules are encapsulated within the cavity, whose nitrogen atoms point toward the Pd^{2+} centers and are stabilized through electrostatic and CH···N interactions ($d_{N\cdots Pd} = d_1 = 3.30$ Å and $d_{N\cdots H} = 2.71$ Å), consistent with related systems [84].

Given the ability of these cages to encapsulate two acetonitrile molecules, we examined their capacity to interact with a series of α,ω-dinitrile alkanes NC–$(CH_2)_n$–CN (*n* = 5, 6, 7, 8, 10, Figure 4a). Although competition with acetonitrile as the solvent was considered, the replacement of two solvent molecules by a single dinitrile guest is expected to be favorable. Indeed, the acetonitrile release provides a negative –TΔS entropic contribution to Gibbs free energy, while the encapsulated dinitrile compounds might establish stabilizing interactions inside the cavity.

Titration experiments were conducted on the $\mathbf{Pd_2(Lb)_4}$ cage in acetonitrile-d_3 at a concentration of C = 0.35 mM. No visible change in the ^1H NMR spectrum was observed upon addition of 100 equivalents of pentanedinitrile ($\mathbf{C_5}$), hexanedinitrile ($\mathbf{C_6}$), decanedinitrile ($\mathbf{C_{10}}$), which indicates that their affinity for the cavity is too weak under these experimental conditions. By contrast, addition of heptanedinitrile ($\mathbf{C_7}$) or octanedinitrile ($\mathbf{C_8}$) produces a new set of sharp signals and the progressive disappearance of those corresponding to the empty cage (Figures 4c, d and S38–S41). The ^1H NMR signals of the encapsulated dinitriles $\mathbf{C_7}$ and $\mathbf{C_8}$ undergo a strong shielding from the aromatic walls surrounding the cavity and their methylene signals appear in the negative region of the spectrum between −0.5 and −2.5 ppm (Figure 4c, d). Overall, this behavior reflects a slow exchange on the NMR timescale and the formation of a well-defined host guest complex. While the complete binding of $\mathbf{C_7}$ requires 80 equivalents of guest at a cage concentration of 0.35 mM, only 2 equivalents of $\mathbf{C_8}$ are sufficient to saturate the cage at the same concentration, reflecting a markedly higher affinity (K_a ($\mathbf{C_8}$) ≈ 970 M^{-1} > K_a ($\mathbf{C_7}$) ≈ 130 M^{-1}, see Supporting Information for details).

Single crystals suitable for x-ray diffraction analysis of the host–guest complexes $\mathbf{C_7}\subset\mathbf{Pd_2(Lb)_4}$ and $\mathbf{C_8}\subset\mathbf{Pd_2(Lb)_4}$ were obtained by vapor diffusion of ethyl acetate into acetonitrile solutions in the presence of $TBAReO_4$ (Figure 3c, d). Both crystallize in the triclinic *P*-1 centrosymmetric space group. The dinitrile chains are fully confined and elongated within the cavity with each terminal nitrogen atom pointing toward one palladium center. The fit of the guest inside the cavity differs for the two homologues.

The $\mathbf{C_8}$ guest exhibits shorter N···Pd contacts (d_1 = 3.23 Å, d_2 = 3.31 Å) compared to $\mathbf{C_7}$ (d_1 = 3.56 Å, d_2 = 3.61 Å), which reflects a better geometric accommodation of the longer chain. In addition, the distances with $\mathbf{C_8}$ are closer to those observed in the case of the two encapsulated acetonitrile molecules (Figure 3a), which further supports the optimal matching between the $\mathbf{C_8}$

guest and the cavity. In addition, this trend is further supported by an analysis of cavity occupation based on volume calculations performed using MoloVol (see SI for computational details) [85]. The internal cavity volume of the **$Pd_2(Lb)_4$** cage was estimated to be 229 Å^3 (Figure S53), while the molecular volumes of guests **C_7** and **C_8** were calculated as 140 Å^3 and 157 Å^3, respectively. These values correspond to occupation parameters of approximately 61% for **C_7** and 68% for **C_8**. While both values deviate from the ~55% occupation parameter proposed by Rebek [86], the higher occupation achieved with C_8 is consistent with a more efficient filling of the cavity and enhanced host–guest contacts. Finally, analysis of the solid-state structures shows that the Pd–Pd separation remains nearly unchanged for the three host cavities, be they occupied by two acetonitrile molecules, **C_7** or **C_8** guests ($d_{Pd–Pd}$ = 17.15, 16.97, and 17.07 Å respectively). This limited variation indicates that the cavity is only weakly flexible and cannot adapt to the size of the guest to maximize the number of stabilizing contacts. The selectivity observed for **C_8** therefore arises from a good host-guest size matching rather than from any conformational adaptation of the host structure.

Cyclic voltammetry studies were conducted on both the ligand **La** and cage **$Pd_2(La)_4$** (See Supporting Information for details). The usual two-electron oxidation behavior of exTTF derivatives is characterized. As expected from the coordination to the metal, the oxidation of the cage is found at a higher potential (E_{ox} = 0.67 V vs. Ag/AgNO$_3$) than the ligand one (E_{ox} = 0.35 V vs. Ag/AgNO$_3$) (Figure S54).

In order to evaluate the impact of the redox state of ligand **La** (neutral or dicationic) over its assembly behavior into a coordination cage, chemical oxidation [87] studies were conducted and monitored by ^{1}H NMR spectroscopy in acetonitrile-d$_3$. Treatment of **La** with two equivalents of phenothiazinium tetrafluoroborate (PTZ$^{\bullet+}$(BF$_4^-$)) [88] in a dichloromethane/acetonitrile mixture (15/85 v/v) afforded the oxidized ligand **La^{ox}** (**$(La^{2+})(BF_4^-)_2$**), which could be isolated by precipitation in Et$_2$O in 86% yield. Attempts to oxidize the **$Pd_2(La)_4$** cage in the same conditions did not afford a well-defined discrete species but instead resulted in complex mixtures. Therefore, the self-assembly behavior of **La^{ox}** was examined in the presence of [Pd(CH$_3$CN)$_4$](BF$_4$)$_2$ in acetonitrile-d$_3$ (Figure 5). Experiments using a 0.5:1 Pd(II):**La^{ox}** ratio did not afford a clean discrete species. By contrast, the use of a 1:1 stoichiometric ratio in both counterparts afforded well-resolved ^{1}H NMR signals after 1 h at 70°C (Figure 5d). Integration of the aromatic region indicated that a dominant species is formed (>80% relative abundance), together with minor undefined species likely arising from incomplete self-assembly or alternative coordination modes. A ^{1}H DOSY NMR experiment confirmed the formation of a single dominant species ($D = 5.7 \times 10^{-10}$ m^2·s^{-1}, Figure 5e) corresponding to a hydrodynamic radius r_H = 11.1 Å, a value which is significantly smaller than that observed for the **$Pd_2(La)_4$** cage (12.3 Å). Importantly, the HRMS analysis performed in acetonitrile at a concentration of 0.07 mM revealed two major peaks corresponding to the [**$Pd_2(La^{ox})_2$**(CD$_3$CN)$_2$F$_2$ – 4BF$_4^-$]$^{4+}$ and [**$Pd_2(La^{ox})_2$**(CD$_3$CN)$_2$F$_2$ – 3BF$_4^-$]$^{3+}$ species, respectively (Figure 5g), consistent with the formation of a $M_2L^{ox}{}_2$ complex. The detected ions indicate that each Pd(II) center remains four-coordinate, adopting a square-planar environment ligated by two nitrogen donors from **La^{ox}**, one acetonitrile molecule, and one fluoride ligand. The

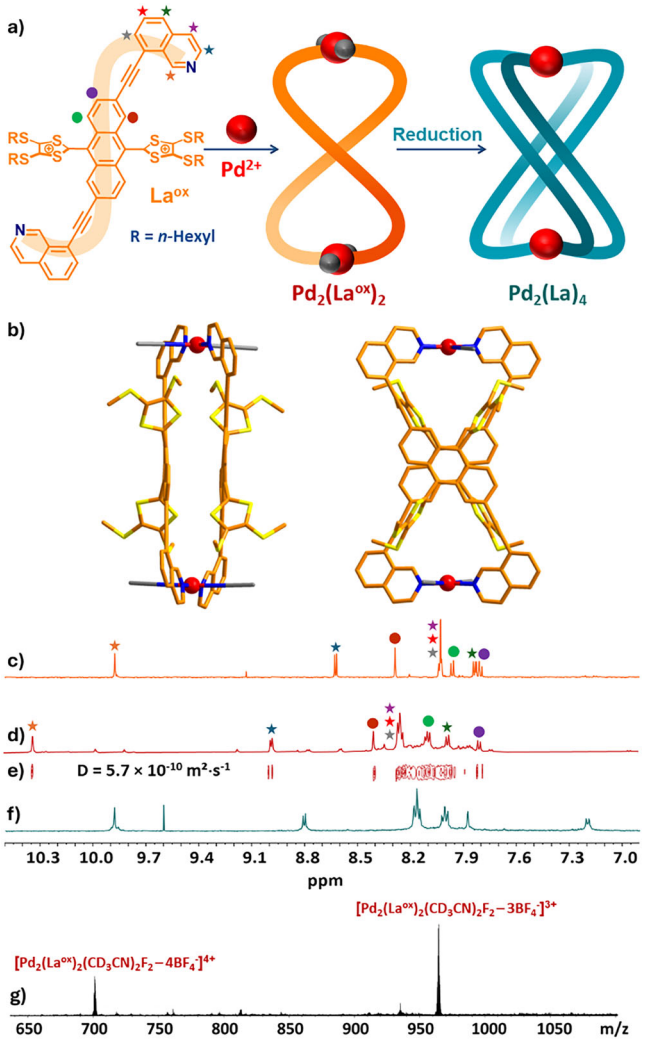

FIGURE 5 | (a) Schematic illustration of the self-assembly between **La^{ox}** and [Pd(CH$_3$CN)$_4$](BF$_4$)$_2$ in acetonitrile-d$_3$ leading to the formation of the oxidized metalla-ring **$Pd_2(La^{ox})_2$** and the subsequent stoichiometry change occurring upon reduction of **$Pd_2(La^{ox})_2$** (grey spheres correspond to coordinated acetonitrile molecules), (b) DFT Optimization of **$Pd_2(La^{ox})_2$**, (c, d, f) ^{1}H NMR spectra recorded in acetonitrile-d$_3$ of **La^{ox}** (c), **$Pd_2(La^{ox})_2$** (d), and **$Pd_2(La)_4$** obtained after reduction of **$Pd_2(La^{ox})_2$** with TDAE (f, e) ^{1}H DOSY NMR spectrum in acetonitrile-d$_3$ of **$Pd_2(La^{ox})_2$** shown in (d, e) ESI-FTICR HRMS spectrum of **$Pd_2(La^{ox})_2$** recorded in acetonitrile-d$_3$ at 0.07 mM.

fluoride likely arises from partial BF$_4^-$ decomposition under the ionization conditions [89], as no Pd-bound fluorine is observed in the ^{19}F NMR spectrum (Figure S32) [90, 91]. While these species are observed in the gas phase, they support a coordination scenario in which the two coordination sites not occupied by **La^{ox}** are filled by solvent and/or anionic ligands. Despite numerous attempts, no single crystal could be obtained from this system. DFT Optimizations were performed (see Supporting Information for computational details) in order to determine the precise geometry of the **$Pd_2(La^{ox})_2$** species and the relative arrangements of the ligands and the Pd(II) centers. The *cis*- and *trans*-[(PdX$_2$)$_2$(La^{ox})$_2$]$^{n+}$ (X = Cl: n = 4 or X = CH$_3$CN: n = 8) geometries were considered, with either chloride ions or acetonitrile molecules occupying the vacant X positions. In

all cases, the *trans* isomer was found to be lower in energy, with energy differences of −142.5 kJ/mol for chloride-coordinated and −30.0 kJ/mol for acetonitrile-coordinated species. The latter exhibits a pronounced steric hindrance arising from the close proximity of the two positively charged **La^{ox}** backbones, which prevents the coordination of two additional ligand molecules to the system. It is worth noting that only few examples of M_2L_2 systems based on pristine palladium complexes have been reported so far and that in these cases, the M_2L_2 formation is rather dictated by steric constraints around the metal centers [34, 92, 93], than by steric hindrance arising from the ligand backbone itself. In other cases, the formation of such M_2L_2 rings has been shown when two of the four coordination sites on the Pd(II) cations are occupied by strongly coordinating anionic ligands such as chloride [94].

The behavior of the resulting **Pd$_2$(La^{ox})$_2$** assembly upon reduction was examined. Tetrakis(dimethylamino)ethylene (TDAE), a two-electron reductant was selected [74, 76, 95, 96]. One equivalent of the reductant was added per constitutive ligand. Noteworthy, the resulting ^{1}H NMR spectrum (Figures 5f and S42 and S43) closely corresponds to the spectrum obtained from the neutral ligand self-assembly indicating the reformation of the **Pd$_2$(La)$_4$** cage. This stoichiometry change remarkably illustrates a ring-to-cage transformation process, in which the **Pd$_2$(La^{ox})$_2$** species is converted into the **Pd$_2$(La)$_4$** cage upon reduction. Concerning this matter, it is worth noting that the **Pd$_2$(La)$_4$** cage is formed despite the presence of an excess of Pd(II) in solution, resulting from the stoichiometric reorganization accompanying the ring-to-cage transformation.

The same methodology was applied for the construction of heteroleptic assemblies incorporating the exTTF motif. Although extensive efforts were devoted to assembling such structures from the neutral ligand **L**, no heteroleptic species could be obtained, despite numerous trials involving ligands expected to display complementary coordination behavior. We therefore investigated the combination of the oxidized **La^{ox}** ligand with a dibenzothiophene-based ligand (**DBT**) (Figure 6a). Notably, **DBT** does not self-assemble with $[Pd(CH_3CN)_4](BF_4)_2$ in acetonitrile because of solubility reasons while it does in DMSO [97]. Heating **DBT** and **La^{ox}** ligands in acetonitrile at 70°C for 12 h furnished a well-resolved ^{1}H NMR spectrum (Figure 6c), significantly different from the homoleptic **Pd$_2$(La^{ox})$_2$** macrocycle (Figure 6b). The spectrum displays high complexity, consistent with the reduced symmetry expected for a heteroleptic assembly. The corresponding ^{1}H DOSY NMR (Figure 6d) shows a single diffusion coefficient ($D = 6.3 \times 10^{-10}$ m^2·s^{-1}) indicating the formation of one discrete species with an estimated hydrodynamic radius of $r_H = 10.0$ Å. The ^{1}H NMR integrals of the isoquinoline protons of **La^{ox}** and the pyridyl protons of **DBT** indicate a 1:2 ligand ratio within the structure. This stoichiometry is further supported by HRMS analysis, which shows intense peaks corresponding to $[$**Pd$_2$(La^{ox})(DBT)$_2$** $- 3BF_4^- + 2CD_3CN]^{3+}$ and $[$**Pd$_2$(La^{ox})(DBT)$_2$** $- 4BF_4^- + 2CD_3CN]^{2+}$, respectively (Figure 6g).

Crystallization attempts were undertaken to characterize the heteroleptic structure. Given its superior crystallization behavior, the ligand **Lb^{ox}**, bearing isobutyl substituents was used instead of **La^{ox}**. Single crystals were obtained by vapor diffusion of diethyl ether into a 0.35 mM acetonitrile solution in the presence of $TBAReO_4$ and the X-ray structure of the expected **Pd$_2$(Lb^{ox})(DBT)$_2$** architecture could be successfully solved (Figure 7a). The observed stoichiometry can be rationalized by the pronounced steric bulk of **Lb^{ox}**, whose anthracene core bears two nearly perpendicular 1,3-dithiolium rings. This steric hindrance prevents a second **Lb^{ox}** ligand from occupying the fourth coordination site on the square-planar Pd(II) centers, meaning that each of them instead binds one acetonitrile molecule. The observed stoichiometry and AAB topology can be rationalized by both i) the pronounced steric bulk of **Lb^{ox}**, whose anthracene core bears two nearly perpendicular 1,3-dithiolium rings, and ii) the complementary binding angles between **DBT** and **Lb^{ox}**. While **DBT** imposes a relatively rigid coordination angle of ca. 77°, the oxidized exTTF-based ligand retains a certain degree of conformational flexibility due to rotation of the isoquinoline donors around the central core, allowing it to adapt its coordination geometry to an angle of ca. 103°, thereby complementing the **DBT** binding angle. Importantly, the steric hindrance imposed by the oxidized $exTTF^{2+}$ core prevents a second oxidized ligand from occupying the fourth coordination site on the square-planar Pd(II) centers, thereby disfavoring the formation of an AABB-type structure and leading instead to coordination of an acetonitrile molecule at the remaining site. The solid-state structure aligns with the ^{1}H NMR data in solution, which display two sets of isoquinoline and pyridyl resonances (Figure 6c), consistent with the reduced symmetry of the heteroleptic cage. In particular, the three ligands bridging the two metal centers form a bowl-like structure. While Pd_2A_2B-type heteroleptic bowls have been reported previously [98], all known examples feature an ABA ligand arrangement, in which two identical A ligands surround the single B ligand, with solvent (or halide) molecules complementing the square-planar coordination spheres of Pd(II) trans to ligand B. In contrast, the ligands reported here adopt an unprecedented AAB arrangement, resulting in a further reduction of the overall symmetry. This difference can be rationalized by the non-linear and complementary coordination vectors of **Lb^{ox}** and **DBT**, in contrast to the typically ligands with colinear vectors involved in ABA-type systems. It is worth noting that crystallographic data on $exTTF^{2+}$ derivatives remain scarce [75, 80, 99, 100–104] and that, to the best of our knowledge have been reported in a unique example of a cage-like structure [76].

Another set of single crystals could also be obtained from a 0.7 mM solution in acetonitrile incorporating $TBAAsF_6$, by vapor diffusion of THF. The corresponding structure could be solved by x-ray diffraction analysis, revealing an original **Pd$_4$(Lb^{ox})$_4$(DBT)$_4$** species with a unique topology (Figures 7b and S55). This assembly consists of two of the heteroleptic **Pd$_2$(Lb^{ox})(DBT)$_2$** bowl-type assemblies, still carrying the two **DBT** units in a *cis* fashion (ligand order AAB), which are connected by two additional bridging **Lb^{ox}** ligands. Each vacant palladium position observed in the parental **Pd$_2$(Lb^{ox})(DBT)$_2$** complex is in this case connected to the isoquinoline moiety of a bridging **Lb^{ox}** ligand. Pd atoms are separated by 13.59 Å within each **Pd$_2$(Lb^{ox})(DBT)$_2$** bowl, while the inter-bowl Pd···Pd distance is 16.28 Å. The internal Pd···Pd···Pd angles alternate between ca. 80° and 100°, resulting in a distorted parallelogram rather than a rectangle. This angular distribution results in two distinct types of corners within the Pd_4 framework. However, the coordination environments of the Pd(II) centers remain very similar overall, with no significant differences in their local

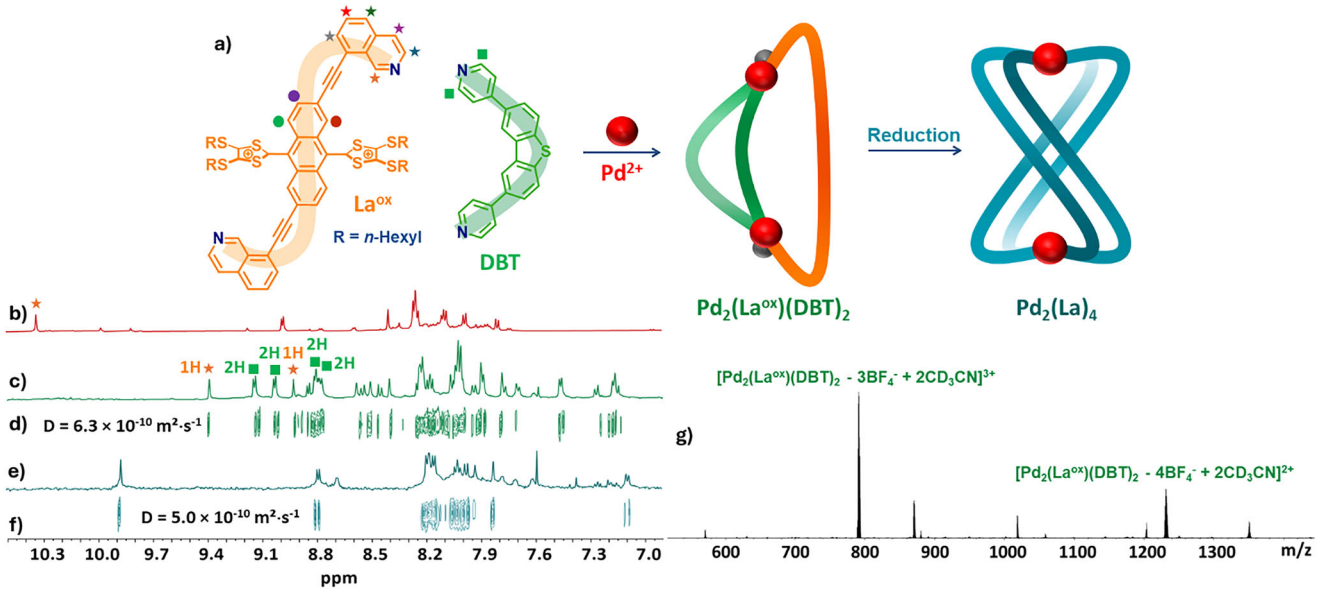

FIGURE 6 | (a) Schematic illustration of the self-assembly between **La^{ox}**, **DBT,** and $Pd(CH_3CN)_4(BF_4)_2$ in acetonitrile-d_3 leading to the formation of the oxidized **Pd$_2$(La^{ox})(DBT)$_2$** heteroleptic structure and the subsequent stoichiometry change occurring upon reduction of **Pd$_2$(La^{ox})(DBT)$_2$** (grey spheres correspond to coordinated acetonitrile molecules), (b, c, e) ^{1}H NMR spectra in acetonitrile-d_3 of **Pd$_2$(La^{ox})$_2$** (b), **Pd$_2$(La^{ox})(DBT)$_2$** (c), and following the reduction of **Pd$_2$(La^{ox})(DBT)$_2$** with TDAE (e), ^{1}H DOSY NMR spectra in acetonitrile-d_3 corresponding d) to the species shown in (c, f) to the species shown in (e) and (g) ESI-FTICR HRMS spectrum of **Pd$_2$(La^{ox})(DBT)$_2$** in acetonitrile-d_3 at 0.07 mM.

square-planar geometries. Attempts to reproduce this species in solution, including experiments at higher concentrations, did not provide evidence for a Pd_4 assembly by NMR spectroscopy, suggesting that its formation may be favored in the solid state by concentration effects, anion templation, and the reduced solvation environment encountered during crystallization Nevertheless, observation of this $M_4L_4L'_4$ species reveals a latent propensity of the system to access higher nuclearity architectures from the availability of vacant coordination sites in the **Pd$_2$(Lb^{ox})(DBT)$_2$** precursor. Previously, such a $M_4L_4L'_4$ stoichiometry has only been described in entirely different arrangements, namely in a heteroleptic pseudo-tetrahedron [105] and in some four-lobed bowl/saddle assemblies [106].

The structures of the redox-active heteroleptic **Pd$_2$(La^{ox})(DBT)$_2$** and **Pd$_2$(Lb^{ox})(DBT)$_2$** architectures have been established in solution and in the solid-state. Their electroactivity was explored to check the impact of the redox-state over their structure. For solubility reasons, these studies were conducted using **Pd$_2$(La^{ox})(DBT)$_2$**. Addition of one equivalent of TDAE per cage unit led to the complete disappearance of the ^{1}H NMR signals which indicates a full disassembly of the heteroleptic architecture and precipitation of the ligands. Heating the mixture allowed reorganization of the components and after 4 h, a ^{1}H NMR spectrum comparable to that of the homoleptic **Pd$_2$(La)$_4$** assembly was obtained (Figures 6e and S44 and S45). The corresponding diffusion coefficient extracted from the ^{1}H DOSY NMR experiment was $D = 5.0 \times 10^{-10}$ m^2·s^{-1} (Figure S46 closely matching that observed for **Pd$_2$(La)$_4$** assembled from neutral **La** ($D = 5.1 \times 10^{-10}$ m^2·s^{-1}). The lower signal intensity observed in the spectrum can be attributed to the stoichiometry of the transformation since formation of one equivalent of **Pd$_2$(La)$_4$** requires four equivalents of **La^{ox}** which reduces the final concentration of the cage. In addition, excess Pd(II) ions remain in solution because the heteroleptic precursor contains more metal than required for formation of the homoleptic product. No resonances of the **DBT** ligand were detected which is consistent with its low solubility in acetonitrile and suggests that it precipitates under these conditions.

This **Pd$_2$(La^{ox})(DBT)$_2$** to **Pd$_2$(La)$_4$** reorganization is assigned to the conformational change occurring upon reduction of the exTTF scaffold to its neutral bent structure, which favors the M_2L_4 nuclearity. To the best of our knowledge, this example corresponds to the first described transformation from a heteroleptic to a homoleptic cage driven by a redox stimulus.

3 | Conclusion

This work establishes exTTF-based ligands as versatile redox responsive components for the construction and transformation of palladium coordination cages. When neutral, the ditopic exTTF-derivative supports the formation of well-defined **Pd$_2$L$_4$** assemblies that display selective recognition for linear α,ω-dinitrile alkanes. On the other hand, oxidation of the exTTF-based ligand to the dicationic state **L^{ox}** offers new opportunities towards new self-assembled structures, by modifying its coordination properties. In that respect, the self-assembly process of **L^{ox}** leads to a **Pd$_2$(L^{ox})$_2$** macrocycle that differs significantly from the parent cage **Pd$_2$L$_4$** obtained from the neutral ligand. The oxidized ligand can also be engaged in heteroleptic self-assemblies upon combining with a dibenzothiophene-based (**DBT**) partner, to produce **Pd$_2$(L^{ox})(DBT)$_2$** or an unprecedented **Pd$_4$(L^{ox})$_4$(DBT)$_4$** parallelogram motif.

Importantly, the reversible nature of these structural changes could be demonstrated, e.g., by restoring the parent homoleptic

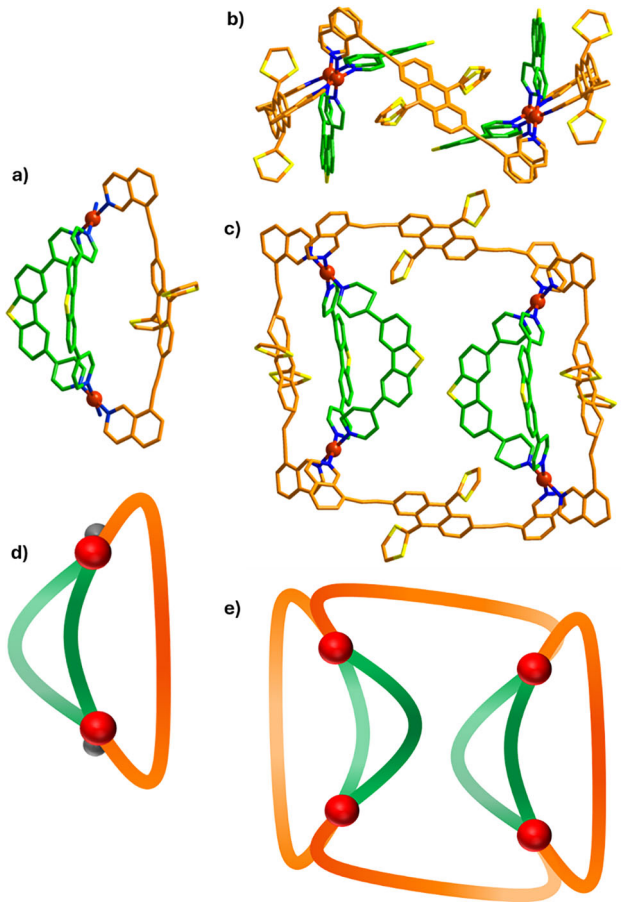

FIGURE 7 | x-Ray crystal structures of (a) $\mathbf{Pd_2(Lb^{ox})(DBT)_2}$, (b) $\mathbf{Pd_4(Lb^{ox})_4(DBT)_4}$ (top view), and (c) $\mathbf{Pd_4(Lb^{ox})_4(DBT)_4}$ (side view); (d, e) corresponding schematic illustrations of (a) and (c), respectively (grey spheres correspond to acetonitrile molecules).

$\mathbf{Pd_2L_4}$ structure upon chemical reduction of the homoleptic $\mathbf{Pd_2(L^{ox})_2}$ system or of the heteroleptic cage $\mathbf{Pd_2(L^{ox})(DBT)_2}$. This sequence of redox-induced transformations outlines the versatility offered by redox-active ligands when aiming at controlling both the composition and the topology of metal organic assemblies.

Author Contributions

Jennifer Bou Zeid: formal analysis, investigation, writing – original draft, methodology. **Jean Nicolas:** investigation, formal analysis, methodology. **Maksym Dekhtiarenko:** investigation, formal analysis. **David Canevet:** formal analysis. **Magali Allain:** formal analysis. **Vincent Carré:** formal analysis. **Frédéric Aubriet:** visualization. **Laura Neukirch:** visualization, methodology. **Elie Benchimol:** visualization, methodology. **Marc Sallé:** conceptualization, writing – review and editing, supervision, methodology, validation. **Guido H. Clever:** conceptualization, writing – review and editing, supervision, funding acquisition, methodology, validation. **Sébastien Goeb:** conceptualization, writing – review and editing, supervision, project administration, funding acquisition, methodology, validation, data curation.

Acknowledgments

The authors gratefully acknowledge for PhD grants, the University of Angers (J. Bou Zeid) and the French Embassy in Kyiv (Ukr) (M. Dekhtiarenko), the EUR LUMOMAT project and the "Investissements d'Avenir" program ANR-18-EURE-0012 as well as the CNRS Chimie for founding an "International Emerging Action" project (RESEARCH) which provided travel support. They also acknowledge the ASTRAL (B. Siegler for NMR spectroscopy) and CRISTAL platforms (SFR MATRIX, Univ. Angers) for their assistance in spectroscopic analyses. Financial support from IR INFRANALYTICS FR2054 for conducting ESI FT-ICR MS measurements at the facility in Metz (LCP-A2MC) is gratefully acknowledged. This work was further supported by the CNRS ЯÉCIPROCS network and was granted synchrotron beamtime by the SOLEIL scientific proposal committee (BAG proposal no. 20231465). The authors gratefully acknowledge Dr. Pierre Fertey for his assistance at the CRISTAL beamline. This work was supported by the Deutsche Forschungsgemeinschaft (DFG) through GRK2376 ("Confinement-Controlled Chemistry", project number 331085229) and under Germany's Excellence Strategy EXC2033, project number 390677874 ("RESOLV"). For the purpose of Open Access, a CC-BY public copyright licence has been applied by the authors to the present document and will be applied to all subsequent versions up to the Author Accepted Manuscript arising from this submission.

Open access publication funding provided by COUPERIN CY26.

Conflicts of Interest

The authors declare no conflicts of interest.

Data Availability Statement

The data that supports the findings of this study are available in the supplementary material of this article.

References

1. Y. Sun, C. Chen, J. Liu, and P. J. Stang, "Recent Developments in the Construction and Applications of Platinum-based Metallacycles and Metallacages via Coordination," *Chemical Society Reviews* 49 (2020): 3889–3919, https://doi.org/10.1039/D0CS00038H.

2. A. E. Martin Diaz and J. E. M. Lewis, "Structural Flexibility in Metal-Organic Cages," *Frontiers in Chemistry* 9 (2021): 706462, https://doi.org/10.3389/fchem.2021.706462.

3. A. J. McConnell, "Metallosupramolecular Cages: From Design Principles and Characterisation Techniques to Applications," *Chemical Society Reviews* 51 (2022): 2957–2971, https://doi.org/10.1039/D1CS01143J.

4. T. Tateishi, M. Yoshimura, S. Tokuda, F. Matsuda, D. Fujita, and S. Furukawa, "Coordination/Metal–organic Cages inside Out," *Coordination Chemistry Reviews* 467 (2022): 214612, https://doi.org/10.1016/j.ccr.2022.214612.

5. D. Tripathy, N. B. Debata, K. C. Naik, and H. S. Sahoo, "Coordination Driven Discrete Metallopolygons and Cages From Unsymmetric Bidentate Ligands," *Coordination Chemistry Reviews* 456 (2022): 214396, https://doi.org/10.1016/j.ccr.2021.214396.

6. H. Zhu, N. M. A. Speakman, T. K. Ronson, and J. R. Nitschke, "Higher-Order Cu I -Based Cages via Subcomponent Self-Assembly," *Accounts of Chemical Research* 58 (2025): 1296–1307, https://doi.org/10.1021/acs.accounts.5c00081.

7. N. B. Debata, D. Tripathy, and D. K. Chand, "Self-Assembled Coordination Complexes From Various Palladium(II) Components and Bidentate or Polydentate Ligands," *Coordination Chemistry Reviews* 256 (2012): 1831–1945, https://doi.org/10.1016/j.ccr.2012.04.001.

8. S. Sharma, M. Sarkar, and D. K. Chand, "Conjoined and Non-Conjoined Coordination Cages With Palladium(II) Vertices: Structural Diversity, Solution Dynamics, and Intermolecular Interactions," *Chemical Communications* 59 (2023): 535–554, https://doi.org/10.1039/D2CC04828K.

9. M. Fujita, M. Tominaga, A. Hori, and B. Therrien, "Coordination Assemblies From a Pd(II)-Cornered Square Complex," *Accounts of Chemical Research* 38 (2005): 369–378, https://doi.org/10.1021/ar040153h.

10. S. Mukherjee and P. S. Mukherjee, "Template-Free Multicomponent Coordination-Driven Self-Assembly of Pd(II)/Pt(II) Molecular Cages," *Chemical Communications* 50 (2014): 2239–2248, https://doi.org/10.1039/C3CC49192G.

11. G. H. Clever and P. Punt, "Cation–Anion Arrangement Patterns in Self-Assembled Pd_2L_4 and Pd_4L_8 Coordination Cages," *Accounts of Chemical Research* 50 (2017): 2233–2243, https://doi.org/10.1021/acs.accounts.7b00231.

12. F. J. Rizzuto, L. K. S. von Krbek, and J. R. Nitschke, "Strategies for Binding Multiple Guests in Metal–organic Cages," *Nature Reviews Chemistry* 3 (2019): 204–222, https://doi.org/10.1038/s41570-019-0085-3.

13. S. Yadav, P. Kannan, and G. Qiu, "Cavity-Based Applications of Metallo-supramolecular Coordination Cages (MSCCs)," *Organic Chemistry Frontiers* 7 (2020): 2842–2872, https://doi.org/10.1039/D0QO00681E.

14. J. E. M. Lewis, "Molecular Engineering of Confined Space in Metal–Organic Cages," *Chemical Communications* 58 (2022): 13873–13886, https://doi.org/10.1039/D2CC05560K.

15. S. Bhattacharyya, M. R. Black, and B. S. Pilgrim, "Encapsulation of Reactive Species Within Metal–organic Cages," *Chemical Science* 16 (2025): 21238–21258, https://doi.org/10.1039/D5SC02081F.

16. A. B. Grommet, M. Feller, and R. Klajn, "Chemical Reactivity Under Nanoconfinement," *Nature Nanotechnology* 15 (2020): 256–271, https://doi.org/10.1038/s41565-020-0652-2.

17. S. Chen and L.-J. Chen, "Metal–Organic Cages: Applications in Organic Reactions," *Chemistry: A European Journal* 4, no. 2 (2022): 494–519, https://doi.org/10.3390/chemistry4020036.

18. R. Ham, C. J. Nielsen, S. Pullen, and J. N. H. Reek, "Supramolecular Coordination Cages for Artificial Photosynthesis and Synthetic Photocatalysis," *Chemical Reviews* 123 (2023): 5225–5261, https://doi.org/10.1021/acs.chemrev.2c00759.

19. Y. Liang, X. Zhou, S. Gopi, and R. Wang, "Distinct Selectivity inside Self-Assembled Coordination Cages," *Frontiers in Chemistry* 11 (2023): 1269471, https://doi.org/10.3389/fchem.2023.1269471.

20. Y. Peng, Z. Su, M. Jin, L. Zhu, Z. J. Guan, and Y. Fang, "Recent Advances in Porous Molecular Cages for Photocatalytic Organic Conversions," *Dalton Transactions* 52 (2023): 15216–15232, https://doi.org/10.1039/D3DT01679J.

21. Z. Ashbridge and J. N. H. Reek, "The Multifaceted Roles of M_nL_{2n} Cages in Catalysis," *Nature Synthesis* 3 (2024): 1197, https://doi.org/10.1038/s44160-024-00606-5.

22. Y. Hao, Y. L. Lu, Z. Jiao, and C. Y. Su, "Photocatalysis Meets Confinement: An Emerging Opportunity for Photoinduced Organic Transformations," *Angewandte Chemie International Edition* 63 (2024): e202317808, https://doi.org/10.1002/ange.202317808.

23. C. García-Simón, M. Garcia-Borràs, L. Gómez, et al., "Sponge-Like Molecular Cage for Purification of Fullerenes," *Nature Communications* 5 (2014): 5557, https://doi.org/10.1038/ncomms6557.

24. C. Fuertes-Espinosa, M. Pujals, and X. Ribas, "Supramolecular Purification and Regioselective Functionalization of Fullerenes and Endohedral Metallofullerenes," *Chemistry* 6 (2020): 3219–3262, https://doi.org/10.1016/j.chempr.2020.11.003.

25. D. Zhang, T. K. Ronson, Y. Q. Zou, and J. R. Nitschke, "Metal–organic Cages for Molecular Separations," *Nature Reviews Chemistry* 5 (2021): 168–182, https://doi.org/10.1038/s41570-020-00246-1.

26. L. Zhang, H. Liu, G. Yuan, and Y.-F. Han, "Chiral Coordination Metallacycles/Metallacages for Enantioselective Recognition and Separation," *Chinese Journal of Chemistry* 39 (2021): 2273, https://doi.org/10.1002/cjoc.202100180.

27. Q. W. Zeng, L. Hu, Y. Niu, et al., "Metal–Organic Cages for Gas Adsorption and Separation," *Chemical Communications* 60 (2024): 3469–3483, https://doi.org/10.1039/D3CC05935A.

28. W. Li, L. Wang, B. E. Keshta, Y. Bi, Y. Zhang, and B. Chen, "Recent Advances on Porous Coordination Cages for Gas Storage and Separation," *Coordination Chemistry Reviews* 545 (2025): 217032, https://doi.org/10.1016/j.ccr.2025.217032.

29. H. Sepehrpour, W. Fu, Y. Sun, and P. J. Stang, "Biomedically Relevant Self-Assembled Metallacycles and Metallacages," *Journal of the American Chemical Society* 141 (2019): 14005–14020, https://doi.org/10.1021/jacs.9b06222.

30. G. Monta-Gonzalez, E. Ortiz-Gomez, R. Lopez-Lima, G. Fiorini, R. Martinez-Manez, and V. Marti-Centelles, "Water-Soluble Molecular Cages for Biological Applications," *Molecules* 29 (2024): 1621, https://doi.org/10.3390/molecules29071621.

31. Y.-P. Wang, Y. Zhang, X.-H. Duan, et al., "Recent Progress in Metal-Organic Cages for Biomedical Application: Highlighted Research During 2018–2023," *Coordination Chemistry Reviews* 501 (2024): 215570, https://doi.org/10.1016/j.ccr.2023.215570.

32. S. Pullen and G. H. Clever, "Mixed-Ligand Metal–Organic Frameworks and Heteroleptic Coordination Cages as Multifunctional Scaffolds—A Comparison," *Accounts of Chemical Research* 51 (2018): 3052–3064, https://doi.org/10.1021/acs.accounts.8b00415.

33. D. Bardhan and D. K. Chand, "Palladium(II)-Based Self-Assembled Heteroleptic Coordination Architectures: A Growing Family," *Chemistry: A European Journal* 25 (2019): 12241–12269, https://doi.org/10.1002/chem.201900831.

34. S. Pullen, J. Tessarolo, and G. H. Clever, "Increasing Structural and Functional Complexity in Self-assembled Coordination Cages," *Chemical Science* 12 (2021): 7269–7293, https://doi.org/10.1039/D1SC01226F.

35. J. L. Algar and D. Preston, "Directing Metallo-supramolecular Assembly Through Complementarity," *Chemical Communications* 58 (2022): 11637–11648, https://doi.org/10.1039/D2CC04464A.

36. P. Howlader and M. Schmittel, "Heteroleptic Metallosupramolecular Aggregates / Complexation for Supramolecular Catalysis," *Beilstein Journal of Organic Chemistry* 18 (2022): 597–630, https://doi.org/10.3762/bjoc.18.62.

37. L. Neukirch and G. H. Clever, "Topological Variety and Self-Sorting in Homo- and Heteroleptic Pd_nL_{2n} Metallo-supramolecular Assemblies," *Chemical Science* 16 (2025): 12242–12276, https://doi.org/10.1039/D5SC03203B.

38. A. K. Bar, S. Raghothama, D. Moon, and P. S. Mukherjee, "Three-Component Self-Assembly of a Series of Triply Interlocked Pd_{12} Coordination Prisms and Their Non-Interlocked Pd_6 Analogues," *Chemistry: A European Journal* 18 (2012): 3199–3209, https://doi.org/10.1002/chem.201102963.

39. D. Preston, J. E. Barnsley, K. C. Gordon, and J. D. Crowley, "Controlled Formation of Heteroleptic $[Pd_2(L_a)_2(L_b)_2]^{4+}$ Cages," *Journal of the American Chemical Society* 138 (2016): 10578–10585, https://doi.org/10.1021/jacs.6b05629.

40. A. M. Johnson and R. J. Hooley, "Steric Effects Control Self-Sorting in Self-Assembled Clusters," *Inorganic Chemistry* 50 (2011): 4671–4673, https://doi.org/10.1021/ic2001688.

41. T. Abe, N. Sanada, K. Takeuchi, A. Okazawa, and S. Hiraoka, "Assembly of Six Types of Heteroleptic Pd_2L_4 Cages Under Kinetic Control," *Journal of the American Chemical Society* 145 (2023): 28061–28074, https://doi.org/10.1021/jacs.3c09359.

42. Y. Liu, S.-H. Liao, W.-T. Dai, et al., "Controlled Construction of Heteroleptic $[Pd_2(L^A)_2(L^B)(L^C)]^{4+}$ Cages: A Facile Approach for Site-Selective Endo-Functionalization of Supramolecular Cavities," *Angewandte Chemie International Edition* 62 (2023): e202217215, https://doi.org/10.1002/ange.202217215.

43. P. Molinska, A. Tarzia, L. Male, K. E. Jelfs, and J. E. M. Lewis, "Diastereoselective Self-Assembly of Low-Symmetry Pd_nL_{2n} Nanocages Through Coordination-Sphere Engineering," *Angewandte Chemie International Edition* 62 (2023): e202315451, https://doi.org/10.1002/ange.202315451.

44. R. G. DiNardi, S. Rasheed, S. S. Capomolla, et al., "Photoswitchable Catalysis by a Self-Assembled Molecular Cage," *Journal of the American Chemical Society* 146 (2024): 21196–21202, https://doi.org/10.1021/jacs.4c04846.

45. E. Benchimol, I. Regeni, B. Zhang, M. Kabiri, J. J. Holstein, and G. H. Clever, "Heteromeric Completive Self-Sorting in Coordination Cage Systems," *Journal of the American Chemical Society* 146 (2024): 6905–6911, https://doi.org/10.1021/jacs.3c14168.

46. E. Benchimol, J. Tessarolo, A. Tarzia, et al., "Adjacent Backbone Interactions Control Self-Sorting of Chiral Heteroleptic $Pd_3A_2B_4$ Isosceles Triangles and $Pd_4A_4C_4$ Pseudo-Tetrahedra," *Chemistry* 12 (2025): 102780, https://doi.org/10.1016/j.chempr.2025.102780.

47. H. Y. Lin, Y. T. Wang, X. Shi, H. B. Yang, and L. Xu, "Switchable Metallacycles and Metallacages," *Chemical Society Reviews* 52 (2023): 1129–1154, https://doi.org/10.1039/D2CS00779G.

48. E. Benchimol, B. T. Nguyen, T. K. Ronson, and J. R. Nitschke, "Transformation Networks of Metal–Organic Cages Controlled by Chemical Stimuli," *Chemical Society Reviews* 51 (2022): 5101–5135, https://doi.org/10.1039/D0CS00801J.

49. S. J. Wezenberg, "Light-switchable Metal-Organic Cages," *Chemistry Letters* 49 (2020): 609–615, https://doi.org/10.1246/cl.200076.

50. A. Diaz-Moscoso and P. Ballester, "Light-Responsive Molecular Containers," *Chemical Communications* 53 (2017): 4635–4652, https://doi.org/10.1039/C7CC01568B.

51. W. Wang, Y. X. Wang, and H. B. Yang, "Supramolecular Transformations Within Discrete Coordination-Driven Supramolecular Architectures," *Chemical Society Reviews* 45 (2016): 2656–2693, https://doi.org/10.1039/C5CS00301F.

52. A. J. McConnell, C. S. Wood, P. P. Neelakandan, and J. R. Nitschke, "Stimuli-Responsive Metal–Ligand Assemblies," *Chemical Reviews* 115 (2015): 7729–7793, https://doi.org/10.1021/cr500632f.

53. I. A. Bhat, D. Samanta, and P. S. Mukherjee, "A Pd_{24} Pregnant Molecular Nanoball: Self-Templated Stellation by Precise Mapping of Coordination Sites," *Journal of the American Chemical Society* 137 (2015): 9497–9502, https://doi.org/10.1021/jacs.5b06628.

54. D. Samanta and P. S. Mukherjee, "Component Selection in the Self-Assembly of Palladium(II) Nanocages and Cage-to-Cage Transformations," *Chemistry: A European Journal* 20 (2014): 12483–12492, https://doi.org/10.1002/chem.201402553.

55. D. Zhang, T. K. Ronson, L. Xu, and J. R. Nitschke, "Transformation Network Culminating in a Heteroleptic $Cd_6L_6L'_2$ Twisted Trigonal Prism," *Journal of the American Chemical Society* 142 (2020): 9152–9157, https://doi.org/10.1021/jacs.0c03798.

56. W. M. Bloch, J. J. Holstein, B. Dittrich, W. Hiller, and G. H. Clever, "Hierarchical Assembly of an Interlocked M_8L_{16} Container," *Angewandte Chemie International Edition* 57 (2018): 5534–5538, https://doi.org/10.1002/ange.201800490.

57. R. Zhu, I. Regeni, J. J. Holstein, et al., "Catenation and Aggregation of Multi-Cavity Coordination Cages," *Angewandte Chemie International Edition* 57 (2018): 13652–13656, https://doi.org/10.1002/ange.201806047.

58. F. J. Rizzuto, J. P. Carpenter, and J. R. Nitschke, "Multisite Binding of Drugs and Natural Products in an Entropically Favorable, Heteroleptic Receptor," *Journal of the American Chemical Society* 141 (2019): 9087–9095, https://doi.org/10.1021/jacs.9b03776.

59. T. Z. Xie, K. J. Endres, Z. Guo, et al., "Controlled Interconversion of Superposed-Bistriangle, Octahedron, and Cuboctahedron Cages Constructed Using a Single, Terpyridinyl-Based Polyligand and Zn^{2+}," *Journal of the American Chemical Society* 138 (2016): 12344–12347, https://doi.org/10.1021/jacs.6b07969.

60. S. Séjourné, A. Labrunie, C. Dalinot, et al., "Chiral Truxene-Based Self-Assembled Cages: Triple Interlocking and Supramolecular Chirogenesis," *Angewandte Chemie International Edition* 63 (2024): e202400961, https://doi.org/10.1002/ange.202400961.

61. J. A. Davies, T. K. Ronson, and J. R. Nitschke, "Twisted Rectangular Subunits Self-Assemble Into a Ferritin-Like Capsule," *Chemistry* 8 (2022): 1099–1106, https://doi.org/10.1016/j.chempr.2022.01.003.

62. S. J. Hu, X. Q. Guo, L. P. Zhou, L. X. Cai, and Q. F. Sun, "Coordination-Assembled Lanthanide-Organic Ln_3L_3 Sandwiches or Ln_4L_4 Tetrahedron: Structural Transformation and Luminescence Modulation," *Chinese Journal of Chemistry* 37 (2019): 657–662, https://doi.org/10.1002/cjoc.201900101.

63. D. Zhang, T. K. Ronson, S. Guryel, J. D. Thoburn, D. J. Wales, and J. R. Nitschke, "Temperature Controls Guest Uptake and Release From Zn_4L_4 Tetrahedra," *Journal of the American Chemical Society* 141 (2019): 14534–14538, https://doi.org/10.1021/jacs.9b07307.

64. L. S. Lisboa, J. A. Findlay, L. J. Wright, C. G. Hartinger, and J. D. Crowley, "A Reduced-Symmetry Heterobimetallic $[PdPtL_4]^{4+}$ Cage: Assembly, Guest Binding, and Stimulus-Induced Switching," *Angewandte Chemie International Edition* 59 (2020): 11101–11107, https://doi.org/10.1002/ange.202003220.

65. M. Dekhtiarenko, S. Pascal, M. Elhabiri, et al., "Reversible pH-Controlled Catenation of a Benzobisimidazole-Based Tetranuclear Rectangle," *Chemistry: A European Journal* 27 (2021): 15922–15927, https://doi.org/10.1002/chem.202103039.

66. M. Han, R. Michel, B. He, et al., "Light-Triggered Guest Uptake and Release by a Photochromic Coordination Cage," *Angewandte Chemie International Edition* 52 (2013): 1319–1323, https://doi.org/10.1002/ange.201207373.

67. H. Lee, J. Tessarolo, D. Langbehn, A. Baksi, R. Herges, and G. H. Clever, "Light-Powered Dissipative Assembly of Diazocine Coordination Cages," *Journal of the American Chemical Society* 144 (2022): 3099–3105, https://doi.org/10.1021/jacs.1c12011.

68. C. Pezzato, C. Cheng, J. F. Stoddart, and R. D. Astumian, "Mastering the Non-Equilibrium Assembly and Operation of Molecular Machines," *Chemical Society Reviews* 46 (2017): 5491–5507, https://doi.org/10.1039/C7CS00068E.

69. K. Cai, L. Zhang, R. D. Astumian, and J. F. Stoddart, "Radical-Pairing-Induced Molecular Assembly and Motion," *Nature Reviews Chemistry* 5 (2021): 447–465, https://doi.org/10.1038/s41570-021-00283-4.

70. A. Iordache, M. Oltean, A. Milet, et al., "Redox Control of Rotary Motions in Ferrocene-Based Elemental Ball Bearings," *Journal of the American Chemical Society* 134 (2012): 2653–2671, https://doi.org/10.1021/ja209766e.

71. R. Kannappan, C. Bucher, E. Saint-Aman, et al., "Viologen-based Redox-Switchable Anion-Binding Receptors," *New Journal of Chemistry* 34 (2010): 1373, https://doi.org/10.1039/b9nj00757a.

72. A. Coskun, J. M. Spruell, G. Barin, et al., "High Hopes: Can Molecular Electronics Realise Its Potential?," *Chemical Society Reviews* 41 (2012): 4827, https://doi.org/10.1039/c2cs35053j.

73. A. Jana, S. Bahring, M. Ishida, et al., "Functionalised Tetrathiafulvalene- (TTF-) Macrocycles: Recent Trends in Applied Supramolecular Chemistry," *Chemical Society Reviews* 47 (2018): 5614–5645, https://doi.org/10.1039/C8CS00035B.

74. V. Croué, S. Goeb, G. Szaloki, M. Allain, and M. Sallé, "Reversible Guest Uptake/Release by Redox-Controlled Assembly/Disassembly of a Coordination Cage," *Angewandte Chemie International Edition* 55 (2016): 1746–1750, https://doi.org/10.1002/ange.201509265.

75. G. Szaloki, S. Krykun, V. Croué, et al., "Redox-Driven Transformation of a Discrete Molecular Cage Into an Infinite 3D Coordination Polymer," *Chemistry: A European Journal* 24 (2018): 11273–11277, https://doi.org/10.1002/chem.201801653.

76. J. B. Zeid, M. Dekhtiarenko, R. Guechaichia, et al., "Redox-Induced Structural Rearrangement in an M_8L_2 Self-Assembly," *Chemistry: A*

European Journal 31 (2025): e202501828, https://doi.org/10.1002/chem.202501828.

77. H. Ube, K. Endo, H. Sato, and M. Shionoya, "Synthesis of Hetero-Multinuclear Metal Complexes by Site-Selective Redox Switching and Transmetalation on a Homo-Multinuclear Complex," *Journal of the American Chemical Society* 141 (2019): 10384–10389, https://doi.org/10.1021/jacs.9b04123.

78. M. Black, S. Bhattacharyya, S. Argent, and B. Pilgrim, "Structural Transformations of Metal–Organic Cages Through Tetrazine-Alkene Reactivity," *Journal of the American Chemical Society* 146 (2024): 28233–28241, https://doi.org/10.1021/jacs.4c08591.

79. F. G. Brunetti, J. L. López, C. Atienza, and N. Martín, "π-Extended TTF: A Versatile Molecule for Organic Electronics," *Journal of Materials Chemistry* 22 (2012): 4188, https://doi.org/10.1039/c2jm15710a.

80. M. R. Bryce, A. J. Moore, M. Hasan, et al., "Electrical and Magnetic Properties and X-Ray Structure of a Highly Conductive 4:1 Complex of Tetracyanoquinodimethane and a Tetrathiafulvalene Derivative," *Angewandte Chemie International Edition* 29 (1990): 1450–1452, https://doi.org/10.1002/ange.199014501.

81. A. J. Moore and M. R. Bryce, "Highly Conjugated π-Electron Donors for Organic Metals: Synthesis and Redox Chemistry of New 1, 3-dithiole and 1, 3-selenathiole Derivatives," *Angewandte Chemie International Edition* 1 (1991): 157–168, https://doi.org/10.1039/P19910000157.

82. V. Croué, S. Krykun, M. Allain, et al., "A Self-Assembled M_2L_4 Cage Incorporating Electron-rich 9-(1, 3-dithiol-2-ylidene) Fluorene Units," *New Journal of Chemistry* 41 (2017): 3238–3241, https://doi.org/10.1039/C7NJ00062F.

83. W. M. Bloch, Y. Abe, J. J. Holstein, C. M. Wandtke, B. Dittrich, and G. H. Clever, "Geometric Complementarity in Assembly and Guest Recognition of a Bent Heteroleptic Cis -$[Pd_2L^A{}_2L^B{}_2]$ Coordination Cage," *Journal of the American Chemical Society* 138 (2016): 13750–13755, https://doi.org/10.1021/jacs.6b08694.

84. H. M. O'Connor, W. J. Tipping, J. Vallejo, et al., "Utilizing Raman Spectroscopy as a Tool for Solid- and Solution-Phase Analysis of Metalloorganic Cage Host–Guest Complexes," *Inorganic Chemistry* 62 (2023): 1827–1832, https://doi.org/10.1021/acs.inorgchem.2c00873.

85. J. B. Maglic and R. Lavendomme, "MoloVol: An Easy-to-Use Program for Analyzing Cavities, Volumes and Surface Areas of Chemical Structures," *Journal of Applied Crystallography* 55 (2022): 1033–1044, https://doi.org/10.1107/S1600576722004988.

86. S. Mecozzi and J. J. Rebek, "The 55% Solution: A Formula for Molecular Recognition in the Liquid State," *Chemistry: A European Journal* 4 (1998): 1016, https://doi.org/10.1002/(SICI)1521-3765(19980615)4:6%3c1016::AID-CHEM1016%3e3.0.CO;2-B.

87. N. G. Connelly and W. E. Geiger, "Chemical Redox Agents for Organometallic Chemistry," *Chemical Reviews* 96 (1996): 877–910, https://doi.org/10.1021/cr940053x.

88. B. K. Bandlish and H. J. Shine, "Ion Radicals. 37. Preparation and Isolation of Cation Radical Tetrafluoroborates by the Use of Nitrosonium Tetrafluoroborate," *The Journal of Organic Chemistry* 42 (1977): 561–563, https://doi.org/10.1021/jo00423a039.

89. I. Regeni, R. Chowdhury, K. Terlinden, et al., "Engineering Soluble Diketopyrrolopyrrole Chromophore Stacks From a Series of Pd(II)-Based Ravels," *Angewandte Chemie International Edition* 62 (2023): e202308288, https://doi.org/10.1002/ange.202308288.

90. V. V. Grushin and W. J. Marshall, *ACS Publications* (2009), https://doi.org/10.1021/ja808975a.

91. N. D. Ball, J. W. Kampf, and M. S. Sanford, "Synthesis and Reactivity of Palladium(II) Fluoride Complexes Containing Nitrogen-donor Ligands," *Dalton Transactions* 39 (2009): 632–640, https://doi.org/10.1039/B914426A.

92. R. Zhu, W. M. Bloch, J. J. Holstein, S. Mandal, L. V. Schäfer, and G. H. Clever, "Donor-Site-Directed Rational Assembly of Heteroleptic Cis -$[Pd_2L_2L'_2]$ Coordination Cages From Picolyl Ligands," *Chemistry: A European Journal* 24 (2018): 12976–12982, https://doi.org/10.1002/chem.201802188.

93. B. Chen, S. Horiuchi, J. J. Holstein, J. Tessarolo, and G. H. Clever, "Tunable Fullerene Affinity of Cages, Bowls and Rings Assembled by Pd II Coordination Sphere Engineering," *Chemistry: A European Journal* 25 (2019): 14921–14927, https://doi.org/10.1002/chem.201903317.

94. R. Zhu, J. Lubben, B. Dittrich, and G. H. Clever, "Stepwise Halide-Triggered Double and Triple Catenation of Self-Assembled Coordination Cages," *Angewandte Chemie International Edition* 54 (2015): 2796–2800, https://doi.org/10.1002/ange.201408068.

95. M. Mahesh, J. A. Murphy, F. LeStrat, and H. P. Wessel, "Reduction of Arenediazonium Salts by Tetrakis(dimethylamino)Ethylene (TDAE): Efficient Formation of Products Derived From Aryl Radicals," *Beilstein Journal of Organic Chemistry* 5 (2009): 1, https://doi.org/10.3762/bjoc.5.1.

96. G. Szaloki, V. Croué, V. Carré, et al., "Controlling the Host–Guest Interaction Mode Through a Redox Stimulus," *Angewandte Chemie International Edition* 56 (2017): 16272–16276, https://doi.org/10.1002/ange.201709483.

97. L. Neukirch, M. D. Kulas, J. J. Holstein, and G. H. Clever, "Non-Templated Assembly of D_{5h}-Symmetric Pd_5L_{10} Rings by Precise Ligand Angle Adjustment," *Chemistry: A European Journal* 30 (2024): e202400132, https://doi.org/10.1002/chem.202400132.

98. B. Chen, J. J. Holstein, A. Platzek, L. Schneider, K. Wu, and G. H. Clever, "Cooperativity of Steric Bulk and H-bonding in Coordination Sphere Engineering: Heteroleptic Pd II Cages and Bowls by Design," *Chemical Science* 13 (2022): 1829–1834, https://doi.org/10.1039/D1SC06931D.

99. A. S. Batsanov, M. R. Bryce, S. B. Lyubchik, and I. F. Perepichka, "An Unexpected TTFAQ Donor–fluorene Acceptor Reaction Resulting in a Novel Salt: 2,6-dihexyloxy-9,10-bis(4,5-dimethyl-1,3-dithiol-2-ylium)-anthracene Bis(2,5,7-trinitro-4-bromo-9-cyanofluorenide) Dioxane Trisolvate," *Acta Crystallographica Section E* 58 (2002): 1106, https://doi.org/10.1107/S1600536802016239.

100. M. R. Bryce, T. Finn, A. S. Batsanov, R. Kataky, J. A. K. Howard, and S. B. Lyubchik, "2,6-Dialkoxy-9,10-bis(1,3-dithiol-2-ylidene)-9,10-dihydroanthracene Derivatives: Synthesis, Electrochemistry and X-ray Crystal Structures of Neutral and Dication Species," *European Journal of Organic Chemistry* 2000 (2000): 1199–1205, https://doi.org/10.1002/1099-0690(200004)2000:7⟨1199::AID-EJOC1199⟩3.0.CO;2-F.

101. C. A. Christensen, A. S. Batsanov, M. R. Bryce, and J. A. Howard, "Molecular Saddles. 7. 1 New 9,10-Bis(1,3-dithiol-2-ylidene)-9,10-dihydroanthracene Cyclophanes: Synthesis, Redox Properties, and X-ray Crystal Structures of Neutral Species and a Dication Salt," *Journal of Organic Chemistry* 66 (2001): 3313–3320, https://doi.org/10.1021/jo001524k.

102. N. Godbert, A. S. Batsanov, M. R. Bryce, and J. A. Howard, "Molecular Saddles. 4. 1 Redox-Active Cyclophanes by Bridging the 9,10-Bis(1,3-dithiol-2-ylidene)-9,10-dihydroanthracene System: Synthesis, Electrochemistry, and X-ray Crystal Structures of Neutral Species and a Dication Salt," *Journal of Organic Chemistry* 66 (2001): 713–719, https://doi.org/10.1021/jo001014q.

103. D. F. Perepichka, M. R. Bryce, I. F. Perepichka, et al., "A (π-Extended Tetrathiafulvalene)–Fluorene Conjugate. Unusual Electrochemistry and Charge Transfer Properties: The First Observation of a Covalent D^{2+}–σ–$A^{\bullet-}$ Redox State 1," *Journal of the American Chemical Society* 124 (2002): 14227–14238, https://doi.org/10.1021/ja012518o.

104. S. Triki, L. Ouahab, D. Lorcy, and A. Robert, "Structure of Anthracenediylidene-bis(1,3-dithiole)–tetracyanoquinodimethane–bis(cyanoformyl)Phenyl-malononitrile Ylide Monohydrate: (Ext-TTF^{2+}).TCNQ.$(Y-)_2$.(H_2O)," *Acta Crystallographica Section C, Crystal Structure Communications* 49 (1993): 1189–1192, https://doi.org/10.1107/S0108270192013283.

105. J. Tessarolo, H. Lee, E. Sakuda, K. Umakoshi, and G. H. Clever, "Integrative Assembly of Heteroleptic Tetrahedra Controlled by Backbone Steric Bulk," *Journal of the American Chemical Society* 143 (2021): 6339–6344, https://doi.org/10.1021/jacs.1c01931.

106. K. E. Ebbert, E. Benchimol, A. Platzek, et al., "Ring-Size Control and Guest-Induced Circularly Polarized Luminescence in Heteroleptic $Pd_3A_3B_3$ and $Pd_4A_4B_4$ Assemblies," *Angewandte Chemie International Edition* 63 (2024): e202413323, https://doi.org/10.1002/ange.202413323.

107. M. Dekhtiarenko, S. Krykun, V. Carré, et al., "Tuning the Structure and the Properties of Dithiafulvene Metalla-assembled Tweezers," *Organic Chemistry Frontiers* 7 (2020): 2040–2046, https://doi.org/10.1039/D0QO00641F.

108. I. Wavefunction, in *Spartan 20 Parallel Suite* (Wavefunction, Inc., 2020).

109. F. Neese, "Software Update: The ORCA Program System—Version 5.0," *WIREs Computational Molecular Science* 12 (2022): e1606, https://doi.org/10.1002/wcms.1606.

Supporting Information

Additional supporting information can be found online in the Supporting Information section.

Supporting File 1: The authors have cited additional references within the Supporting Information [107–109].

Supporting File 2: ange72437-sup-0002-DataFile.zip